SIMULATION OF METEOROID-VELOCITY IMPACT BY USE OF DENSE PROJECTILES

by Robert H. Morrison

Ames Research Center
Moffett Field, Calif.

1. Report No. NASA TN D-5734	2. Government Accession No.	3. Recipient's Catalog No.
4. Title and Subtitle SIMULATION OF METEOROID-VELOCITY IMPACT BY USE OF DENSE PROJECTILES		5. Report Date April 1970
		6. Performing Organization Code
7. Author(s) Robert H. Morrison		8. Performing Organization Report No. A-3315
9. Performing Organization Name and Address NASA Ames Research Center Moffett Field, Calif., 94035		10. Work Unit No. 124-09-15-02-00-21
		11. Contract or Grant No.
		13. Type of Report and Period Covered Technical Note
12. Sponsoring Agency Name and Address National Aeronautics and Space Administration Washington, D.C. 20546		
		14. Sponsoring Agency Code

15. Supplementary Notes

16. Abstract

A technique is described for simulating the impacts of semi-infinite targets by low-density, low-fineness ratio cylinders at meteoroid velocities by impacting high-density, low-velocity projectiles. Conditions for simulation are stated and embodied in a model forming the basis of the technique. The feasibility of the technique is experimentally investigated by simulating the impacts of semi-infinite aluminum targets by polyethylene plastic cylinders of various low-fineness ratios and the same velocity of 11.3 km/sec. The penetrations were simulated at lower velocities to within 10 percent by impacting aluminum, steel, nickel, and copper projectiles, but only to within 30 percent by impacting platinum projectiles. In application of the technique, the impacts of semi-infinite aluminum targets by cylinders of polyethylene and porous aluminum (0.44 g/cm^3) at velocities of 15.2 and 22 km/sec, respectively, were simulated.

17. Key Words Suggested by Author(s) Meteoroids Hypervelocity Impact Projectile Simulation	18. Distribution Statement Unclassified - Unlimited		
19. Security Classif. (of this report) Unclassified	20. Security Classif. (of this page) Unclassified	21. No. of Pages 34	22. Price* $3.00

SYMBOLS

A_i area of portion i of interface

c   speed of sound

d   diameter of cylinder

E   specific internal energy

I   interface between impacting materials

i   portion of interface inside boundary defined by points of intersection of cylinder's radial rarefaction with interface

J   impulse given to target material in time t_2 by pressures acting at portion i of interface

K   constant

l length of cylinder

m   mass of cylinder

P   penetration (maximum depth of crater) measured from undisturbed target surface

p   pressure

R   rarefaction (head of rarefaction wave)

r   radial coordinate

S   shock wave

t   time measured from instant of impact

t_1 time for shock wave to reach rear face of impacting cylinder

t_2 time at which axial rarefaction reaches interface

U   velocity of one-dimensional shock wave relative to undisturbed medium

u   mass velocity behind one-dimensional shock wave relative to undisturbed medium

v   velocity of cylinder at impact

x   axial coordinate

$\eta = \dfrac{\rho}{\rho_0}$

θ dimensionless parameter defined by equation (9)

$\mu = \eta - 1$

ρ density

Subscripts

H   Hugoniot state

o   initial state

p   projectile or cylinder material

r   radial direction

t   target material

x   axial direction

μ impact case of low-density cylinder

σ impact case of simulating projectile

SIMULATION OF METEOROID-VELOCITY IMPACT BY USE OF

DENSE PROJECTILES

By Robert H. Morrison

Ames Research Center

SUMMARY

A technique is described for simulating the impacts of semi-infinite targets by low-density, low-fineness-ratio cylinders at meteoroid velocities by impacting high-density, low-velocity projectiles. Conditions for simulation are stated and embodied in a model forming the basis of the technique. The feasibility of the technique is experimentally investigated by simulating the impacts of semi-infinite aluminum targets by polyethylene plastic cylinders of various low-fineness ratios and the same velocity of 11.3 km/sec. The penetrations were simulated at lower velocities to within 10 percent by impacting aluminum, steel, nickel, and copper projectiles, but only to within 30 percent by impacting platinum projectiles. In application of the technique, the impacts of semi-infinite aluminum targets by cylinders of polyethylene and porous aluminum (0.44 g/cm^3) at velocities of 15.2 and 22 km/sec, respectively, were simulated.

INTRODUCTION

The simulation of meteoroid impact has, for the most part, been beyond the capabilities of light-gas-gun facilities. The highest impact velocity attained in these facilities, 11.3 km/sec, is just at the lower end of the meteoroid velocity spectrum of 11 to 73 km/sec (ref. 1).

This velocity (ref. 2) was obtained with a low-density, plastic cylinder that impacted an aluminum target. Calculations indicate that the initial pressure produced in the target material by this impact is less than that produced by much slower, higher density projectiles. This observation suggests that with the proper dimensions and velocities, higher density projectiles could generate pressure pulses in the target material which would approximate that generated by the plastic cylinder impacting at a velocity exceeding 11.3 km/sec, and the projectiles thereby could simulate, to some degree, its impact damage at presently unattainable velocities. In the same manner, the impacts of low-density meteoroids at higher velocities could be simulated.

As a step toward this goal, design criteria are herein proposed for the dimensions and velocities of dense projectiles to simulate the impacts of low-density, low-fineness-ratio cylinders at meteoroid velocities. The model in which these criteria are given and the results of experiments designed to

test the technique are presented. Penetration data are included for effectively semi-infinite 2024-T351 aluminum targets impacted by aluminum, steel, nickel, copper, and platinum cylinders at velocities ranging from 4.41 to 8.35 km/sec.

THEORETICAL CONSIDERATIONS

Early Stages of Hypervelocity Impact

During the early stages of hypervelocity impact, much of the process can be analyzed in terms of highly simplified flows: one-dimensional flow behind a normal shock and expansion-wave heads propagating from free surfaces through material at uniform pressure. If enough of the impulse given to the target occurs during this "simple" part of the flow, it should be possible to define conditions for impact equivalence between projectiles of widely different physical properties.

The axisymmetric, hypervelocity impact of a semi-infinite target by a low-fineness-ratio cylinder is depicted at the instant of impact in figure 1. The cylinder's velocity v, diameter d, length l, and initial density ρ_{op}, which in the general case is different from the initial density of the target, ρ_{ot}, are indicated. The orthogonal coordinate system x - r is fixed in the target with the x axis coinciding with the axis of the cylinder. From the instant of impact, the materials of both the cylinder and the target will be compressed to very high pressures by shock waves. These pressures, greatly exceeding the strengths of both materials, will start a nonsteady, three-dimensional compressible flow.

The salient features of this compressible flow at two early times after impact are shown in figure 2, for a case where the speed of sound at the initial impact (Hugoniot) pressure in the cylinder material is less than that of the target material.

In figure 2(a) the wave pattern of this flow in a cross-sectional plane through the x axis has been estimated for a time soon after impact. The shock waves S_p and S_t are shown propagating away from the interface I between the materials of the cylinder and target, compressing these respective materials. Also shown are the heads R_{rp} and R_{rt} of the radial rarefaction waves, which start inward at the instant of impact from the surface of the cylinder. Since the speed of sound in the target material is greater, the radial rarefaction in this material precedes that in the cylinder material along the interface. Because pressure waves are transmitted across the interface, expansion Mach waves are formed in the cylinder material. However, in figure 2, the cylinder's radial rarefaction is shown as though its propagation were unaffected by these expansions. When the speed of sound at impact is greater in the cylinder material, Mach waves are generated in the target material instead. (In similar materials, no such waves are formed.) A radial rarefaction and the associated Mach waves form a boundary, inside of which the flow is still one-dimensional and the two shock waves and the

2

interface are planar. Outside this boundary, the flow is three-dimensional and the shock waves and interface are curved.

At a later time, the shock S_p will have reflected from the cylinder's rear face as a rarefaction. The wave pattern at this time is estimated in figure 2(b). Shown again are the radial rarefactions in the target material, which by this time are approaching the x axis, having penetrated most of the one-dimensional flow. Inside the region bounded by the radial expansion system, the axial rarefaction head, R_{xp} remains planar.

The material and wave motions occurring along the x axis during these early stages of the impact are better shown in the wave diagram of figure 3. The shock wave S_p propagates through the cylinder and, upon encountering the cylinder's rear face at time t_1, is reflected as the axial rarefaction R_{xp}, which starts the isentropic release of the material from the Hugoniot pressure. Subsequently, at time t_2, the axial rarefaction overtakes the interface I. For the fineness ratios being considered, the axial rarefaction arrives at this point before either of the radial rarefactions.

The cylinder velocity v and the wave arrival times t_1 and t_2 may all be related to the impacting cylinder's dimensions and the one-dimensional flow parameters (see appendix A). These parameters are the speeds U and u, relative to the undisturbed medium, of the shock wave and the compressed material, respectively, and the speed of sound c_H in this compressed material at pressure p_H. These parameters may be calculated for various materials and any given pressure p_H, as indicated in appendix B. The relations are

$$v = u_p + u_t \tag{1}$$

$$t_1 = l/U_p \tag{2}$$

$$t_2 = l(1/U_p + 1/\eta_{Hp}c_{Hp}) \tag{3}$$

where

$$\eta_H = U/(U - u)$$

The flow parameters u, U, and c_H must be evaluated for the materials of the cylinder (subscript p) and the target (subscript t) at the same Hugoniot pressure.

Simulation Model

It is postulated that the initial part of the pressure pulse generated in a semi-infinite target by the hypervelocity impact of a low-density, low-fineness-ratio cylinder can be simulated and that this impact can thereby be simulated with the impact of a slower, higher density cylindrical projectile if the following conditions are met. The Hugoniot pressure p_H and the

arrival time t_2 of the axial rarefaction at the interface are to be the same for both cases. Furthermore, the same impulse J is to be given to the target material in this time by pressures acting at the portion i of the interface inside the boundary that is delineated by the points of intersection of the cylinder's radial rarefaction with this interface. To delineate this boundary, the assumptions are made that the precedence of a target's radial rarefaction causes a negligible reduction in the pressure at the interface from the Hugoniot pressure p_H before the arrival of the cylinder's radial rarefaction, and that this precedence therefore has a negligible effect on the latter wave's propagation. Thus, the portion i of the interface is approximately planar and at a constant pressure p_H. The above conditions for simulation may be written, respectively, as

$$p_{H\sigma} = p_{H\mu} \tag{4}$$

$$t_{2\sigma} = t_{2\mu} \tag{5a}$$

$$J_\sigma = J_\mu \tag{6a}$$

where the subscripts μ and σ denote the impact cases of the lower density cylinder and the simulating projectile, respectively.

The preceding conditions and assumptions are sufficient to specify the velocity, length, and fineness ratio of a simulating projectile in terms of these same quantities for the low-density cylinder and the one-dimensional flow parameters. The velocity of this projectile is derived by substituting equation (1) into the equation

$$u_{t\sigma} = u_{t\mu} \tag{7a}$$

which is implied by the condition of equation (4). The velocity thus obtained is

$$v_\sigma = v_\mu + u_{p\sigma} - u_{p\mu} \tag{7b}$$

The length of this projectile is obtained from equations (5a) and (3) as

$$\ell_\sigma = \frac{\left(1/U_p + 1/\eta_{Hp}c_{Hp}\right)_\mu}{\left(1/U_p + 1/\eta_{Hp}c_{Hp}\right)_\sigma} \ell_\mu \tag{5b}$$

Its fineness ratio is derived from equation (6a) by first developing an expression for the impulse J as follows. If A_i is the area of the portion i of the interface, the impulse J may be expressed as

$$J = \int_0^{t_2} p_H A_i \, dt = p_H \int_0^{t_2} A_i \, dt$$

However, the area A_i is given by

4

$$A_i = \frac{\pi}{4}\left(d - 2c_{Hp}t\right)^2 \tag{8}$$

Substituting this expression for A_i into the one for J, performing the integration, and rearranging the resultant expression yields

$$J = \frac{\pi}{4}\, p_H t_2^3 c_{Hp}^2\, \theta$$

where θ is a dimensionless parameter defined as

$$\theta = \left[\frac{1}{c_{Hp}\left(1/U_p + 1/n_{Hp}c_{Hp}\right)\left(l/d\right)} - 1\right]^2 + \frac{1}{3} \tag{9}$$

If the latter expression for J is substituted and the conditions of equations (4) and (5a) are applied, equation (6a) becomes

$$\theta_\sigma = \left(c_{Hp\mu}/c_{Hp\sigma}\right)^2 \theta_\mu \tag{6b}$$

By use of the identity of equation (9), the projectile's fineness ratio is found to be

$$\left(l/d\right)_\sigma = \left[c_{Hp\sigma}\left(1/U_p + 1/n_{Hp}c_{Hp}\right)_\sigma\left(1 + \sqrt{\theta_\sigma - 1/3}\right)\right]^{-1} \tag{10}$$

where θ_σ is related to the low-density cylinder's properties by equation (6b).

In summary, the velocity, length, and fineness ratio of a cylindrical projectile to simulate the impact of a low-density, low-fineness-ratio cylinder are given, respectively, by the equations

$$v_\sigma = v_\mu + u_{p\sigma} - u_{p\mu} \tag{7b}$$

$$l_\sigma = \frac{\left(1/U_p + 1/n_{Hp}c_{Hp}\right)_\mu}{\left(1/U_p + 1/n_{Hp}c_{Hp}\right)_\sigma}\, l_\mu \tag{5b}$$

$$\left(l/d\right)_\sigma = \left[c_{Hp\sigma}\left(1/U_p + 1/n_{Hp}c_{Hp}\right)_\sigma\left(1 + \sqrt{\theta_\sigma - 1/3}\right)\right]^{-1} \tag{10}$$

where

$$\theta_\sigma = \left(\frac{c_{Hp\mu}}{c_{Hp\sigma}}\right)^2 \left\{\left[\frac{1}{c_{Hp\mu}\left(1/U_p + 1/n_{Hp}c_{Hp}\right)_\mu \left(l/d\right)_\mu} - 1\right]^2 + \frac{1}{3}\right\}$$

5

and

$$\eta_H = U/(U - u)$$

EXPERIMENTS

The experimental investigation consisted of two parts. First, the applicability of the preceding simulation relationships was determined by simulating the impact of the previously mentioned plastic cylinder of reference 2. The cylinder was polyethylene with a density of 0.95 g/cm^3 and a fineness ratio of 1/3. To examine somewhat more generally the applicability of the simulation technique, the impacts of polyethylene cylinders with lower fineness ratios and the same velocity (11.3 km/sec) were also simulated. In the second part of the experimental investigation, an impact of the 1/3-fineness-ratio polyethylene cylinder was simulated at a higher velocity of 15.2 km/sec. For each simulation, the penetration (target-crater depth) so obtained was compared with that estimated from

$$P/d = 0.34(l/d)^{1/4}v^{2/3} \tag{11}$$

(ref. 3), which is applicable to the hypervelocity impact of 2024-T351 aluminum by polyethylene cylinders with fineness ratios from 1/6 to 1.

To simulate the impacts in the first part of the experimental investigation, the following projectile materials were used: 2024-T351 aluminum, AISI 1018 steel, pure nickel, OFHC copper, and pure platinum. For the second part, only OFHC copper was used. The velocities of the various simulating projectiles for yielding Hugoniot pressures of 1.05 and 1.70 megabars and thus simulating polyethylene impacting at 11.3 and 15.2 km/sec, respectively, are listed in table 1. The velocities were calculated for each pressure from equation (7b) by substituting the velocity of polyethylene for v_μ and the values calculated as indicated in appendix B for $u_{p\sigma}$ and $u_{p\mu}$.

Projectiles of these materials were machined with diameters near 5 mm and various low-fineness ratios. The diameters and lengths were measured to within 0.06 and 0.6 percent, respectively. The projectiles were then launched, sabot-mounted, at the required velocities in the ballistic ranges employed in the investigations of references 2 and 4. The light gas guns of these ranges were equipped with rifle barrels, which imparted spin to the projectiles to ensure attitude near zero angle of attack and separation of the segmented sabots. Spark shadowgraphs taken at numerous stations on these ranges provided orthogonal views of the projectiles in flight and thereby gave condition and attitude data. The angles of attack did not exceed 5° and therefore were in the range found in reference 3, for which any anomalies due to angles of attack are outweighed by the inherent variation in crater formation. These shadowgraphs, together with the measurements for intervals of time and distance between the stations, made possible in each case a determination of the impact velocity to within 1 percent.

6

The targets were of the same material (2024-T351 aluminum) and size (10 × 10 × 5.1 cm) as those of references 2 and 3. The depths of the resultant craters were measured relative to the undisturbed target face to within 0.6 percent by an especially adapted dial indicator.

RESULTS AND DISCUSSION

The pertinent data and the results of the simulation tests are given in tables 2 and 3, respectively. In table 3, the dimensionless penetration $(P/d)_\sigma$, corresponding to the velocity v_σ, together with the density $\rho_{o\sigma}$, length l_σ, and fineness ratio $(l/d)_\sigma$, is listed for each simulating projectile. The velocity v_μ, length l_μ, and fineness ratio $(l/d)_\mu$ of the polyethylene cylinder whose penetration P_μ was simulated by each projectile and the penetration of this projectile normalized with respect to that estimated for the corresponding polyethylene cylinder P_σ/P_μ are also listed. In addition, the maximum deviation of the dimensionless penetration P/d is given for each projectile from a curve described by an equation of the form $P/d = Kv^{2/3}$ and fitted to the data by the method of least squares. This relation between penetration and impact velocity was shown to apply for hypervelocity impact up to the 11.3 km/sec in reference 2. The maximum deviation of P/d, within 3 percent for each case where several data points were obtained, shows that this relation adequately describes the data over the velocity range tested. In each case, the equation was used to estimate $(P/d)_\sigma$ at the simulating velocity v_σ. The length l_μ and $(l/d)_\mu$ were calculated by means of equations (5b) and (10), respectively; whereas the normalized penetration was calculated from the equation

$$\frac{P_\sigma}{P_\mu} = \frac{1}{0.34} \frac{(1/U_p + 1/\eta_{Hp}c_{Hp})_\mu}{(1/U_p + 1/\eta_{Hp}c_{Hp})_\sigma} \frac{(l/d)_\mu^{3/4}}{(l/d)_\sigma} \frac{(P/d)_\sigma}{v_\mu^{2/3}} \tag{12}$$

which is derived by substituting equations (5b) and (11) into the identity

$$\frac{P_\sigma}{P_\mu} = \frac{(P/d)_\sigma}{(P/d)_\mu} \frac{(l/d)_\mu}{(l/d)_\sigma} \frac{l_\sigma}{l_\mu}$$

In using equation (12) for the smallest fineness ratio aluminum projectile and its corresponding 0.118-fineness ratio polyethylene cylinder, it was assumed that the l/d relation of equation (11) still held.

For each simulating projectile, the normalized penetration P_σ/P_μ is plotted versus the fineness ratio $(l/d)_\mu$ of the corresponding polyethylene cylinder in figure 4. This figure and table 3 show that the aluminum, steel, nickel, and copper projectiles, having fineness ratios from 0.0816 to 0.224, simulated with good accuracy (to within 10 percent) the penetrations of their corresponding polyethylene cylinders, having fineness ratios from 0.118 to

7

0.313. However, poor results were obtained with the platinum projectiles, since the penetrations were deeper than those of their corresponding polyethylene cylinders by as much as 30 percent.

The impacts of the steel, nickel, copper, and platinum simulating projectiles correspond to the previously discussed case of figure 2, where the speed of sound in the target material at high pressure is greater than that of the cylinder material, and therefore the radial rarefaction in the target precedes that in the cylinder along the interface. For the impacts of the corresponding polyethylene cylinders, the opposite is true. The fineness ratio of each simulating projectile and its corresponding polyethylene cylinder, however, was sufficiently low that the axial rarefaction reached the point on the axis at the interface before either of the radial rarefactions.

The poor results obtained with the platinum projectiles cannot be attributed solely to experimental errors since these errors were no larger than those for the smallest fineness ratio aluminum projectile, which simulated closely the polyethylene impact. Nor is the variation in crater depths, as represented by the maximum deviation of P/d from the fitted curve, large enough to account for the 20 to 30 percent deeper penetration of platinum since this deviation was only 1 percent. Although a different equation of state was used in calculating the one-dimensional flow parameters for platinum (see appendix B), its use also is not thought to be solely responsible for the much deeper penetrations.

Rather, the poor results obtained with the platinum projectiles are probably due to the radial and axial expansions of projectile material being much slower in each of these cases subsequent to time t_2. The slower radial expansion is evident from table 4 where it is shown that, despite selection of fineness ratio and length to duplicate the impulse J of the impact of the 1/3-fineness-ratio polyethylene cylinder, the area of the one-dimensional flow at time t_2 is much larger than in the polyethylene case. The same is true for simulation with copper and aluminum, but to a lesser extent. The slower axial expansion, on the other hand, is evident if one considers the reflection of the axial rarefaction from the interface, which must occur for impacts of dissimilar materials because of the acoustic mismatch present there. The much greater acoustic impedance of the platinum causes a large negative reflection of the axial rarefaction, which, in turn, causes the initial pressure decay at the portion i of the interface to be much slower than for the polyethylene case where a positive reflection occurs. The pressure decay is also slower for simulations with copper and aluminum, but again to a lesser extent. The much slower radial and axial expansions in the platinum cause the shock pressure in the aluminum target to be sustained to greater depths, thus producing greater penetrations. This suggests the inadequacy of the simple criteria for projectile dimensions when the physical properties of the projectile materials differ vastly from those of the low-density cylinder. However, the use of such projectile materials in simulating actual meteoroid impacts to develop a design criterion would result in an overestimation of meteoroid penetration ability and, therefore, lead to a conservative design for meteoroid protection.

8

Profiles of the craters produced by the simulating projectiles impacting at Hugoniot pressures near 1.05 megabar are depicted in figure 5. As can be seen from the photographs, the crater shapes are more conical than hemispherical, which was the result obtained in reference 2 for the impact of the high speed polyethylene cylinder (see fig. 6). However, in comparison, the craters made by the platinum projectiles have relatively flat bottoms. The craters for the aluminum, copper, and platinum projectiles of fineness ratios 0.224, 0.151, and 0.122, respectively, (see figs. 5(a), (d), and (e)) nearly simulate the impact of the 1/3-fineness-ratio polyethylene cylinder of reference 2. Their profiles are compared in figure 7. Except for the platinum impact crater, these craters are very similar to that produced by the polyethylene cylinder.

The results of the tests indicate the feasibility of using slower moving but more dense projectiles to simulate the impacts of semi-infinite targets by low-density, low-fineness-ratio cylinders at meteoroid velocities. It is emphasized that the technique is restricted to impacts on semi-infinite targets, but an analogous treatment of thin-target impact might prove useful. In particular, the technique can be used for simulating the impacts of low-fineness-ratio cylinders of polyethylene and porous aluminum at presently unattainable meteoroid velocities.

In this application of the technique, the impact of a 1/3-fineness-ratio polyethylene cylinder at 15.2 km/sec was simulated by a copper projectile. The results are given in table 3 and figure 8. The simulated penetration agrees with that estimated by equation (11) to the same accuracy as that obtained for the lower velocity simulation. This agreement implies that the velocity exponent of this equation applies to impacts of polyethylene at velocities up to 15 km/sec. It is interesting that the shape of the simulated impact crater in figure 8 is more hemispherical than conical, which is a result just opposite to that obtained for the lower velocity simulation.

As a further application of the technique, the impacts of porous aluminum cylinders with density of 0.44 g/cm^3 that are simulated by (1) the high-velocity polyethylene cylinder of reference 2 and (2) the highest velocity copper projectile of table 3 were determined. The impacts of particles with this density are of interest since various astronomers have suggested densities of about this value for cometary meteoroids (ref. 5) which are thought to be porous. The results are given in table 5, which lists the velocity v_μ, length l_μ, fineness ratio $(l/d)_\mu$, the dimensionless penetration $(P/d)_\mu$, and the ratio of the penetration to the cube root of the mass $(P/m^{1/3})_\mu$ for the simulated porous aluminum cylinders. These quantities were calculated from the data for the simulating projectiles by using the values of the one-dimensional flow parameters for the porous aluminum as obtained from the appendixes of references 6 and 7. Also listed in table 5 for comparison is the ratio $(P/m^{1/3})_\mu$ for the impact of semi-infinite aluminum by an aluminum cylinder with the same porosity and velocity as the simulated cylinders, but with a fineness ratio of unity. The ratio in this case was determined from the theoretical results of reference 6.

The velocities of the porous aluminum projectiles, the impacts of which were simulated by the referenced polyethylene cylinder and the copper projectile, represent gains of 59 and 95 percent, respectively, over the velocity of the referenced cylinder. However, the penetration simulated by copper probably overestimates that which would actually be produced by the porous aluminum cylinder since the physical properties of these two materials differ vastly. In fact, the penetration simulated by copper is about 10 percent greater than that predicted by extrapolating from the penetration simulated by polyethylene according to the relation $P/d \propto v^{2/3}$. Nevertheless, using these simulated penetrations in determining required meteoroid protection for spacecraft should lead to a conservative design.

The ratios $(P/m^{1/3})_\mu$ for the simulated porous aluminum cylinders do not necessarily apply to impacts of cylinders of other fineness ratios, but these ratios do agree rather well with those obtained theoretically for the unit-fineness-ratio cylinders. The maximum difference is only about 10 percent, which was obtained for the impact simulated by copper. If, for the porous aluminum cylinders, $(P/m^{1/3})_\mu$ is indeed not a function of fineness ratio, then there is no shape effect for these cylinders similar to that found for the impacts of polyethylene cylinders in reference 3.

CONCLUSIONS

The results of the tests indicate that the penetrations into semi-infinite aluminum targets by polyethylene cylinders of various low-fineness ratios impacting at 11.3 km/sec were simulated to within 10 percent by the impacts at lower velocities of aluminum, steel, nickel, and copper projectiles, but only to within 30 percent by the impacts of platinum projectiles. From these results it is concluded that the technique is feasible for simulating the impacts of semi-infinite targets by low-density, low-fineness-ratio cylinders at meteoroid velocities, within certain limits. The principal limitation seems to be that the sound speed in the simulating projectile cannot be too small compared to the sound speed in the cylinder, the impact of which is to be simulated. The impacts of semi-infinite 2024-T351 aluminum targets by cylinders of polyethylene and porous aluminum (0.44 g/cm^3) at velocities of 15.2 km/sec and 22 km/sec, respectively, were simulated by this technique.

Ames Research Center
    National Aeronautics and Space Administration
        Moffett Field, Calif., 94035, Nov. 5, 1969

APPENDIX A

DERIVATIONS

The velocity v can be related to the one-dimensional flow parameters if the boundary conditions of equal pressure and velocity are applied on either side of the planar interface (see fig. 2). These conditions are

$$p_{Hp} = p_{Ht} = p_H \tag{A1}$$

and

$$v - u_p = u_t \tag{A2}$$

The first condition requires that the mass velocities u_p and u_t be evaluated at the same pressure p_H, and the second yields the relation

$$v = u_p + u_t \tag{A3}$$

for the velocity.

The relations for the arrival times t_1 and t_2 can be derived in a manner similar to that indicated in reference 8.

APPENDIX B

CALCULATION OF ONE-DIMENSIONAL FLOW PARAMETERS

The parameters of the one-dimensional flow behind a planar shock wave are obtained by application of the conservation laws of mass, momentum, and energy across this wave. By choosing a coordinate system fixed in the undisturbed medium, one may derive the familiar Rankine-Hugoniot equations

$$\eta_H = \rho_H/\rho_o = U/(U - u) \tag{B1}$$

$$p_H - p_o = \rho_o u U \tag{B2a}$$

$$E_H - E_o = \left(p_H + p_o\right)\left(1/\rho_o - 1/\rho_H\right)/2 \tag{B3a}$$

where U and u are the speeds, relative to the undisturbed medium, of the shock wave and the shock-compressed material, respectively. The symbols p, ρ, and E represent, respectively, the pressure, density, and specific internal energy of the material at the initial state (subscript o) and at the shocked Hugoniot state (subscript H). For convenience, E_o may be chosen to be zero; and since for hypervelocity impact $p_H \gg p_o$, the last two equations may be approximated as

$$p_H = \rho_o u U \tag{B2b}$$

$$E_H = \frac{p_H}{2\rho_o} \frac{\eta_H - 1}{\eta_H} \tag{B3b}$$

where the definition of equation (B1) has been substituted.

To solve for the four unknowns η_H, p_H, u, and U, a fourth equation, the equation-of-state of the material, is required. In this report, two forms for this equation were used for nonporous materials. The first of these is the semiempirical equation of Tillotson (ref. 9),

$$p(\rho,E) = \left(a + \frac{b}{E/E_o\eta^2 + 1}\right)E\rho + A\mu + B\mu^2 \tag{B4}$$

where $\eta = \rho/\rho_o$, $\mu = \eta - 1$, and a, b, A, B, and E_o are constants. The values of these constants for various materials are listed in table 6, as given by or adapted from references 9 and 10. This formulation represents a best-fit interpolation between calculations from Thomas-Fermi-Dirac theory

for very high pressures and experimental data at low pressures and is estimated to be accurate to within 5 percent of the Hugoniot pressure for pressures below 5 megabars. The second form of the equation of state (Enig, ref. 11) is based on the "p-u mirror-image" approximation. This equation,

$$4Sp\left(\rho, u_H\right) = \left(4Sp_H + \rho_o C_o^2\right)\exp\left[-4S\rho_o\left(1/\rho - 1/\rho_H\right)\right] - \rho_o C_o^2 \tag{B5}$$

(the notation for S in ref. 11 is a) makes use of the linear approximation

$$U = C_o + Su \tag{B6}$$

(C_o and S are empirical constants), which is applicable for many materials over a large pressure range. The values of these constants for various materials and the range of pressures for which they are applicable, as obtained from reference 12, are listed in table 7.

The flow parameters may all be expressed in terms of the Hugoniot pressure p_H by equations, the convenience of which is determined by the equation of state used. If Tillotson's equation is used, the most convenient equations for these parameters are

$$u = \left(\frac{\eta_H - 1}{\eta_H} \frac{p_H}{\rho_o}\right)^{1/2} \tag{B7a}$$

$$U = \left(\frac{\eta_H}{\eta_H - 1} \frac{p_H}{\rho_o}\right)^{1/2} \tag{B8a}$$

$$c_H^2 = f_1\left(p_H, \eta_H\right)$$

$$= \frac{A + 2B\mu_H}{\rho_o} + \frac{p_H}{\rho_o}\left\{a\left(\frac{\eta_H + 1}{2\eta_H}\right) + b\eta_H^2\left[\frac{3\mu_H^2 p_H/4\rho_o E_o + \eta_H^3\left(1 + \mu_H/2\right)}{\left(\mu_H p_H/2\rho_o E_o + \eta_H^3\right)^2}\right]\right\} \tag{B9a}$$

where c_H is the speed of sound in the shocked medium at the Hugoniot pressure. The first two equations are obtained by solving equations (B1) and (B2b). The last equation is found by applying the definition of the speed of sound, $c^2 = (\partial p/\partial \rho)_S$, to equation (B4) and substituting into the result equation (B3b) and the thermodynamic relation $(\partial E/\partial \rho)_S = p/\rho^2$. The Hugoniot

13

pressure p_H in these equations is given by equation (B4) as $p_H = p_H(\rho_H, E_H)$. However, if equations (B1) and (B3b) are substituted into this equation for p_H, η_H is obtained implicitly as $\eta_H = \eta_H(p_H)$. Therefore, the flow parameters are functions only of the Hugoniot pressure

$$u = u(p_H) \tag{B7b}$$

$$U = U(p_H) \tag{B8b}$$

$$c_H = c_H(p_H) \tag{B9b}$$

If Enig's equation is used, the most convenient equations for these parameters are

$$u = -C_0/2S + \sqrt{(C_0/2S)^2 + p_H/\rho_0 S} \tag{B10}$$

$$U = C_0 + Su \tag{B6}$$

$$c_H = (U + Su)(U - u)/U \tag{B11}$$

Equation (B10) is obtained by solving equations (B2b) and (B6), whereas equation (B11) is obtained by applying the definition of c to equation (B5) and substituting into the result equations (B1) and (B10).

For the simulation tests, the one-dimensional flow parameters were calculated by using Tillotson's equation for polyethylene, 2024-T351 aluminum, AISI 1018 steel, nickel, and OFHC copper and by using Enig's equation for platinum. For porous aluminum of density of 0.44 g/cm³, the values of these parameters were obtained from the appendixes of references 6 and 7. The use of Enig's equation for platinum was necessary since the constants of Tillotson's equation for this material were not available. The constants used for polyethylene were adapted from those given in reference 10 for a slightly lower density polyethylene and are listed in table 6.

In addition, it was assumed that the equations of state for aluminum and steel alloys could be approximated by those for pure aluminum and pure iron, respectively. This approximation is good in the case of the aluminum alloy, since the values of u, U, and c_H calculated for this material at $p_H = 1.000$ megabar by using Enig's equation are within 2 percent of the corresponding values calculated by using both this equation and that of Tillotson for pure aluminum.

Using Enig's equation to calculate the one-dimensional flow parameters for Al, Fe, Ni, Cu, and W at $p_H = 1.000$ megabar gives values that agree well with those calculated by using Tillotson's equation. For each of these materials, the values of u and the values of c_H, calculated by using the two different equations of state, agree to within 1 percent and 3 percent,

14

respectively. Furthermore, the values of U agree to within 1 percent for each of these materials except Fe, for which the values agree to within only 6 percent. The agreement of these values provides confidence in the values of the parameters for Pt, for which only Enig's equation was used.

REFERENCES

1. Cosby, William A.; and Lyle, Robert G.: The Meteoroid Environment and Its Effects on Materials and Equipment. NASA SP-78, 1965.

2. Denardo, B. Pat: Penetration of Polyethylene into Semi-Infinite 2024-T351 Aluminum up to Velocities of 37,000 Feet Per Second. NASA TN D-3369, 1966.

3. Denardo, B. Pat: Projectile Shape Effects on Hypervelocity Impact Craters in Aluminum. NASA TN D-4953, 1968.

4. Nysmith, C. Robert; and Summers, James L.: An Experimental Investigation of the Impact Resistance of Double-Sheet Structures at Velocities to 24,000 Feet Per Second. NASA TN D-1431, 1962.

5. Whipple, Fred L.: On Meteoroids and Penetration. J. Geophys. Res., vol. 68, no. 17, Sept. 1, 1963, pp. 4929-4939.

6. Bjork, R. L.; Kreyenhagen, K. N.; and Wagner, M. H.: Analytical Study of Impact Effects as Applied to the Meteoroid Hazard. NASA CR-757, 1967.

7. Rosenblatt, Martin; Kreyenhagen, Kenneth N.; and Romine, Dennis W.: Analytical Study of Debris Clouds Formed by Hypervelocity Impacts on Thin Plates. Final Technical Report AFML-TR-68-266, Shock Hydrodynamics, Inc., December 1968.

8. Fowles, G. R.: Attenuation of the Shock Wave Produced in a Solid by a Flying Plate. J. Appl. Phys., vol. 31, no. 4, April 1960, pp. 655-661.

9. Tillotson, J. H.: Metallic Equations of State for Hypervelocity Impact. GA-3216 (AF29(601)-4759), General Atomic Div. of General Dynamics, July 1962.

10. Walsh, J. M.; Johnson, W. E.; Dienes, J. K.; Tillotson, J. H.; and Yates, D. R.: The Theory of Hypervelocity Impact. Summary Report GA-5119 (DA-04-495-AMC-116(X)), General Atomic Div. of General Dynamics, March 1964.

11. Enig, Julius W.: A Complete E, P, V, T, S Thermodynamic Description of Metals Based on the P, U Mirror-Image Approximation. J. Appl. Phys., vol. 34, no. 4, Pt. 1, April 1963, pp. 746-754.

12. Van Thiel, M., ed.: Compendium of Shock Wave Data. Sections A-1, A-2. UCRL-50108, vols. I and II, Lawrence Radiation Lab., U. of Calif., Livermore, Calif., June 1966.

TABLE 1.- SIMULATING PROJECTILE VELOCITIES
FOR IMPACTS ON ALUMINUM TARGETS

Projectile material	Velocity, v_σ, km/sec, at	
	$p_H = 1.05$ Mb	$p_H = 1.70$ Mb
Polyethylene	$=V_\mu=11.3$	$=V_\mu=15.2$
2024-T351 Al	7.40	10.3
AISI 1018 steel	5.64	7.83
Ni	5.39	7.53
OFHC Cu	5.48	7.61
Pt	4.67	6.50

TABLE 2.- SUMMARY OF PERTINENT EXPERIMENTAL DATA

Round	Projectile						Penetration, P, mm	Projectile	
	Material	Density, ρ_{op}, g/cm³	Diameter, d, mm	Length, ℓ, mm	Mass, m, g	Velocity, v, km/sec		Mean length, mm	Mean fineness ratio
568 *	Polyethylene	0.95	5.702	1.8	0.0453	11.3	7.54	1.8	0.32
989	2024-T351 Al	2.77	5.075	.411	.0233	7.40	5.23	.414	.0816
994			5.075	.417	.0233	5.96	4.57		
995			5.072	.417	.0232	8.19	5.56		
997			5.075	.411	.0230	8.35	5.69		
990			5.072	.818	.0467	7.55	6.50	.822	.162
991			5.075	.826	.0469	5.86	5.44	.822	.162
J-108			5.080	1.10	.0616	6.56	6.38	1.10	.216
J-117			5.090	1.09	.0611	6.76	6.55		
J-119			5.085	1.09	.0605	6.95	6.81		
J-122			5.080	1.10	.0615	6.75	6.68		
J-123					.0613	6.97	6.73		
J-124					.0616	6.61	6.40		
J-125					.0610	7.27	6.96		
J-126					.0610	7.22	6.83		
J-127					.0614	6.85	6.66		
J-203			5.362	1.20	.0752	6.70	6.88	1.20	.224
J-114	AISI 1018 Steel	7.84	5.080	.686	.1079	5.05	7.11	.687	.136
J-115		7.84		.688	.1075	5.31	7.29	.687	
J-116	Ni	8.86		.691	.1209	5.06	7.49	.691	
J-197	OFHC Cu	8.90		.460	.0812	5.17	6.30	.460	.0905
J-213				.518	.0917	5.44	6.83	.526	.104
J-214				.533	.0953	5.56	7.14	.526	.104
J-109				.645	.1122	5.80	7.87	.654	.129
J-110			5.105	.650	.1102	6.03	7.98		
J-111			5.080	.655	.1088	5.85	7.75		
J-112				.665	.1123	5.28	7.24		
J-259				.655	.1178	6.06	8.28		
J-198			4.821	.729	.1180	5.42	7.75	.735	.152
J-205				.744	.1208	5.56	7.92		
J-206				.739	.1201	5.74	8.08		
SR-196				.732	.1190	6.89	9.27		
SR-197			4.811	.732	.1181	7.20	9.52		
SR-198			4.821	.742	.1200	7.63	9.88		
SR-200			4.811	.726	.1171	7.82	9.88		
J-211	Pt	21.42	5.090	.483	.2098	4.72	9.35	.481	.0945
J-249				.475	.2048	4.62	9.02		
J-251				.485	.2086	4.70	9.27		
J-207			4.559	.551	.1923	5.37	10.2	.550	.121
J-209				.546	.1912	4.41	9.12		
J-210				.554	.1935	4.69	9.42		

*From reference 2

TABLE 3.– RESULTS OF SIMULATION TESTS

	Simulating projectile						Polyethylene[a] cylinder			Normalized penetration, P_σ/P_μ
Material	Density, $\rho_{o\sigma}$, g/cm³	Velocity, v_σ, km/sec	Length, ℓ_σ, mm	Fineness ratio, $(\ell/d)_\sigma$	Dimensionless penetration, $(P/d)_\sigma$	Maximum deviation of P/d, percent	Velocity, v_μ, km/sec	Length, ℓ_μ, mm	Fineness ratio, $(\ell/d)_\mu$	
2024-T351 Al	2.77	7.40	0.414	0.0816	1.03	1	11.3	0.614	0.118	1.0
			.822	.162	1.26	1		1.22	.229	1.0
			1.10	.216	1.38	2		1.63	.302	1.0
			1.20	.224	1.37[b]	--		1.78	.313	1.0
AISI 1018 steel	7.84	5.64	.687	.136	1.50	0		1.59	.272	1.1
Ni	8.86	5.39	.691	.136	1.54[b]	--		1.60	.274	1.1
OFHC Cu	8.90	5.48	.460	.0905	1.29[b]	--		1.11	.195	1.0
P_t	21.42	4.67	.526	.104	1.37	1		1.27	.221	1.0
			.654	.129	1.48	3		1.58	.268	1.1
P_t	21.42	4.67	.735	.152	1.64	1		1.77	.311	1.1
			.481	.0945	1.81	1		1.54	.254	1.2
OFHC Cu	8.90	7.61	.550	.121	2.06	1		1.77	.314	1.3
			.735	.152	2.04	1	15.2	1.86	.324	1.1

[a] Density of 0.95 g/cm³

[b] Based on only one data point

TABLE 4.– RATIO OF AREA A_i AT TIME t_2 FOR EACH PROJECTILE SIMULATING IMPACT OF 1/3-FINENESS RATIO POLYETHYLENE CYLINDER AT 11.3 km/sec TO THAT OF THIS CYLINDER

Simulating projectile			Area ratio, $\left(\dfrac{A_{i\sigma}}{A_{i\mu}}\right)_{t_2}$
Material	Density, $\rho_{o\sigma}$, g/cm³	Fineness ratio, $(\ell/d)_\sigma$	
2024-T351 Al	2.77	0.224	2.28
OFHC Cu	8.90	.152	4.79
Pt	21.42	.121	6.44

TABLE 5.- SIMULATED IMPACTS OF POROUS ALUMINUM (0.44 g/cm^3) CYLINDERS

	Simulating projectile			Porous aluminum cylinder					
Material	Velocity, v_σ, km/sec	Length, l_σ, mm	Fineness ratio, $(l/d)_\sigma$	Velocity, v_μ, km/sec	Length, l_μ, mm	Fineness ratio, $(l/d)_\mu$	Dimensionless penetration, $(P/d)_\mu$	$(P/m^{1/3})_\mu$, cm/g$^{1/3}$	$(P/m^{1/3})_\mu$ for $(l/d)_\mu = 1$, cm/g$^{1/3}$
Polyethylene	11.3	1.8	0.32	18	2.5	0.47	1.4	2.6	2.6[a]
OFHC Cu	7.61	0.735	.152	22	2.6	.47	1.8	3.3	3.0[a]

[a]From theoretical results of reference 6

TABLE 6.- CONSTANTS FOR TILLOTSON'S EQUATION OF STATE

Material	a	b	A, Mb	B, Mb	E_0, Mb-cm^3/g	Normal density, ρ_0, g/cm^3	Sources
Polyethylene	0.6	2.0	0.075	0.02	0.07	0.92	References 9 and 10
W	.5	1.04	3.08	2.50	.225	19.17	
Cu	.5	1.5	1.39	1.10	.325	8.90	
Fe	.5	1.5	1.279	1.05	.095	7.86	
Al	.5	1.63	.752	.65	.050	2.70	
Be	.55	.62	1.1734	.55	.175	1.85	
Ti	.5	.60	1.03	.50	.070	4.51	
Ni	.5	1.33	1.912	1.50	.090	8.86	
Mo	.5	1.02	2.713	1.65	.045	10.20	
Th	.4	.86	.531	.50	.025	11.68	
Polyethylene	.6	2.0	.075	.002	.07	.95	Assumed

TABLE 7.- EMPIRICAL CONSTANTS IN THE EQUATION $U = C_0 + Su$
[From ref. 12]

| Material	Normal density, ρ_0, g/cm^3	C_0, km/sec	S	Applicable pressure range, Mb
W	19.17	4.005	1.268	0.395 - 2.074
Cu	8.90	3.958	1.497	.883 - 1.444
Fe	7.86	3.768	1.655	.43 - 1.967
Al	2.71	5.38	1.35	.693 - 1.972
Al 2024	2.785	5.355	1.345	.015 - 1.022
Ni	8.86	4.646	1.445	1.009 - 1.491
Pt	21.43	3.646	1.535	.322 - 2.718
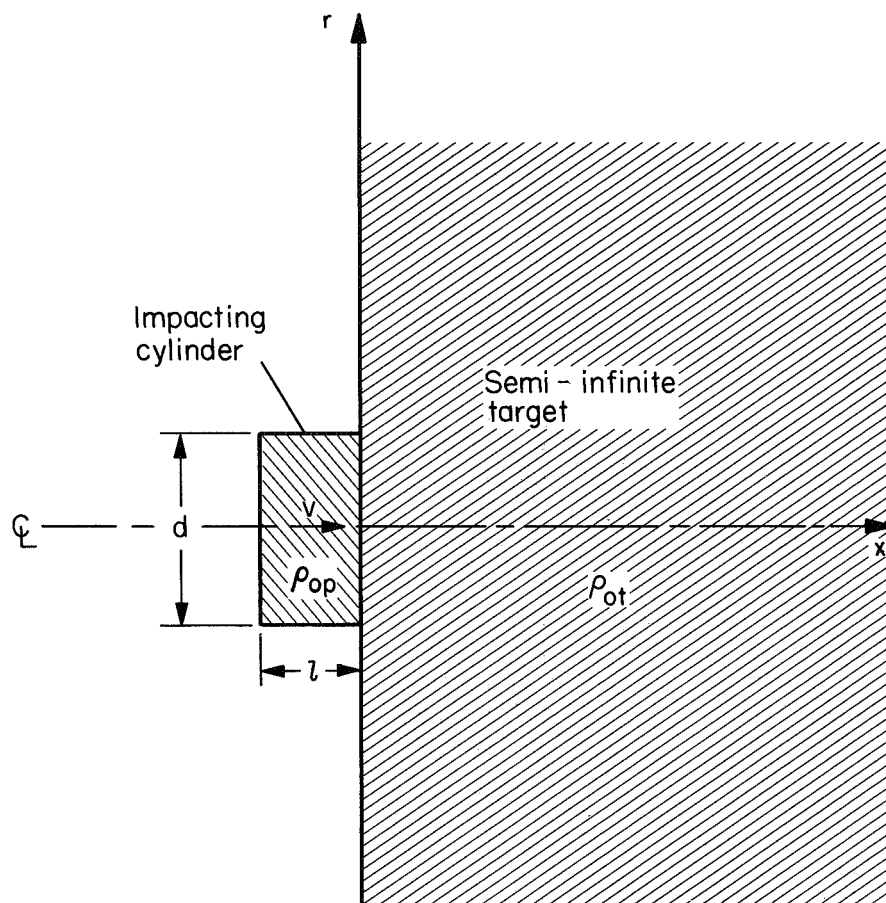
Figure 1.- Axisymmetric, hypervelocity impact of semi-infinite target by low-fineness-ratio cylinder of dissimilar material.
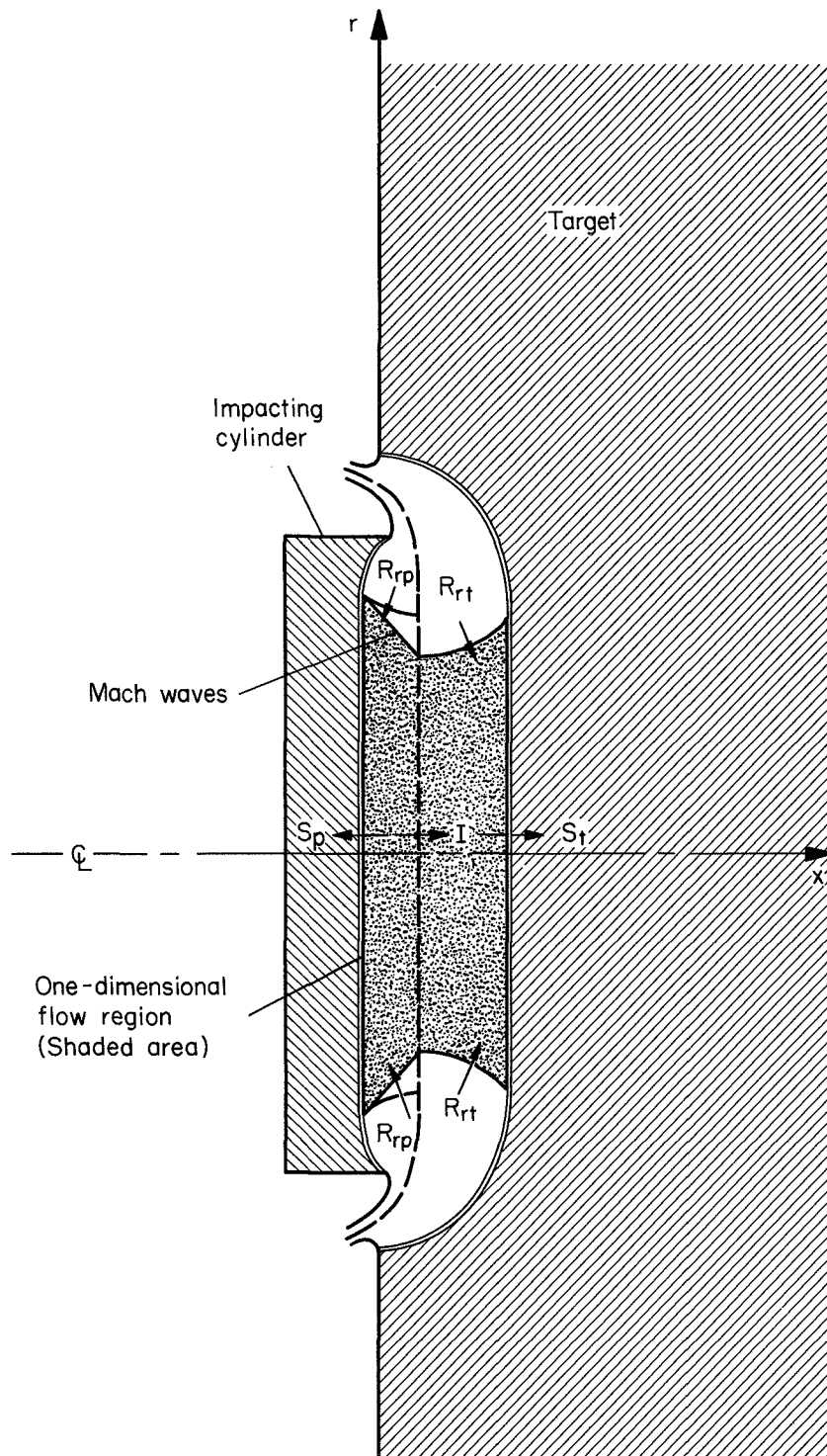
(a) At time soon after impact.

Figure 2.- Estimated wave pattern for axisymmetric, hypervelocity impact of semi-infinite target by low-fineness-ratio cylinder (dissimilar material).
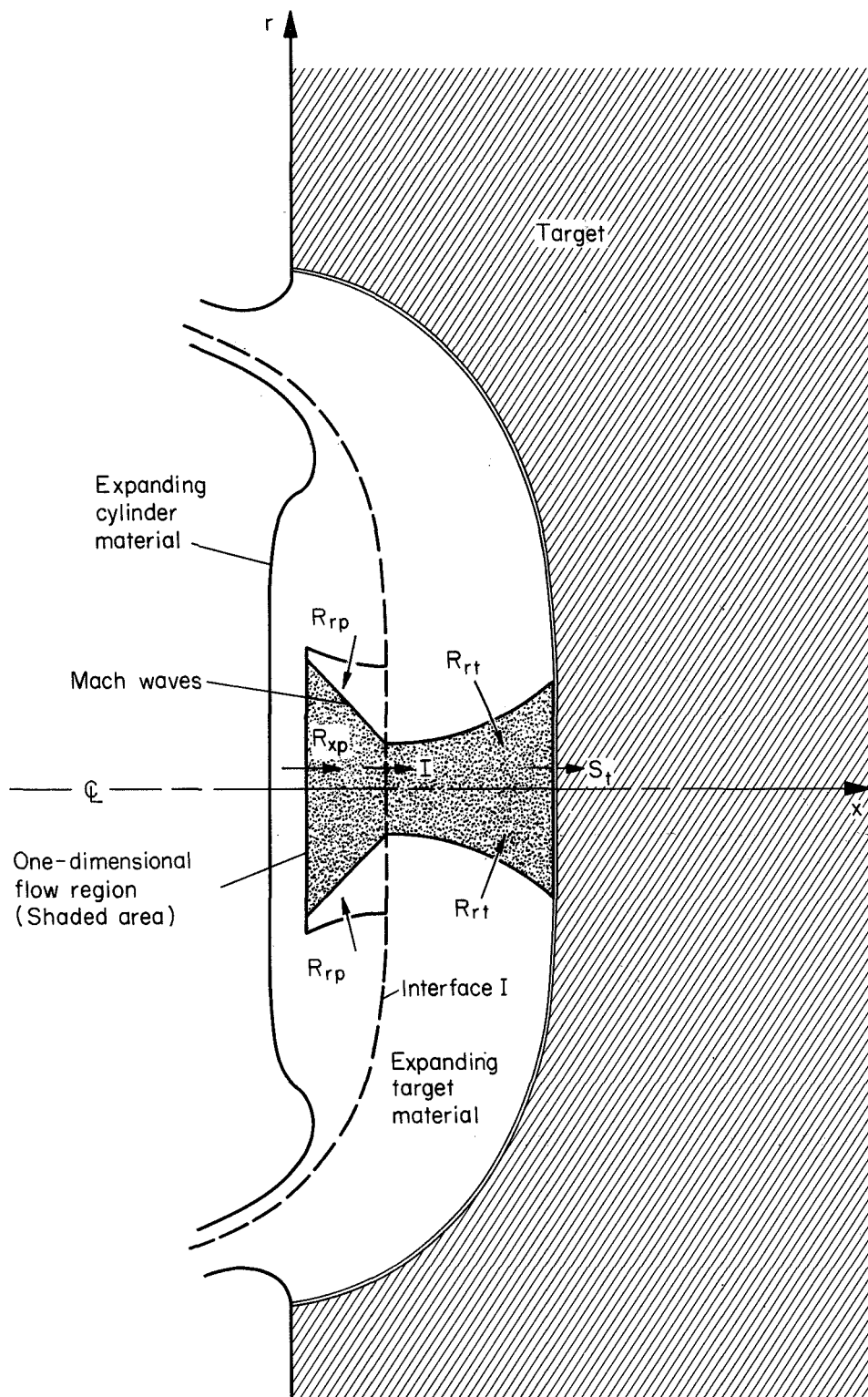
(b) At time soon after reflection of shock wave S_p from cylinder's rear face.
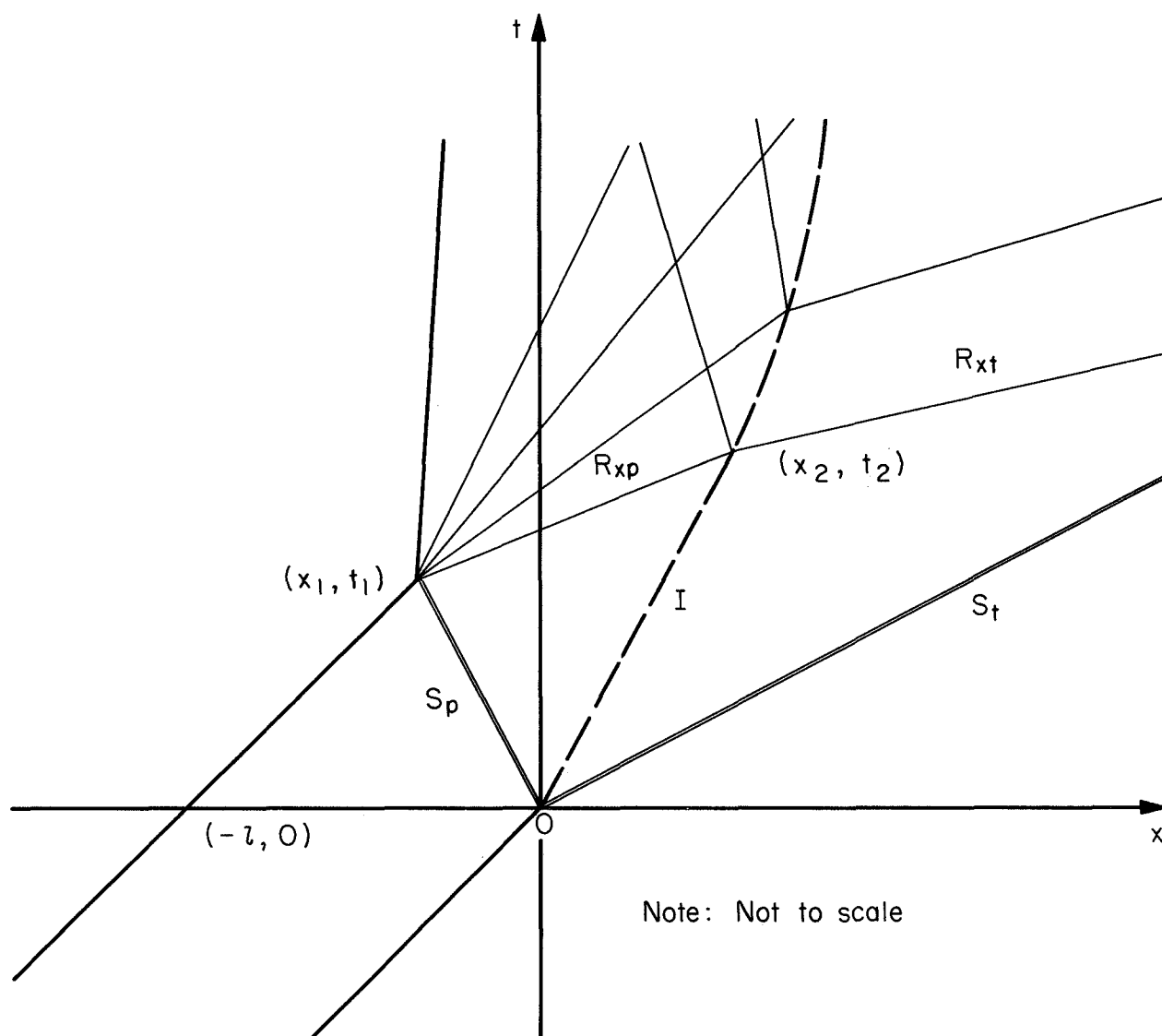
Figure 2.- Concluded.

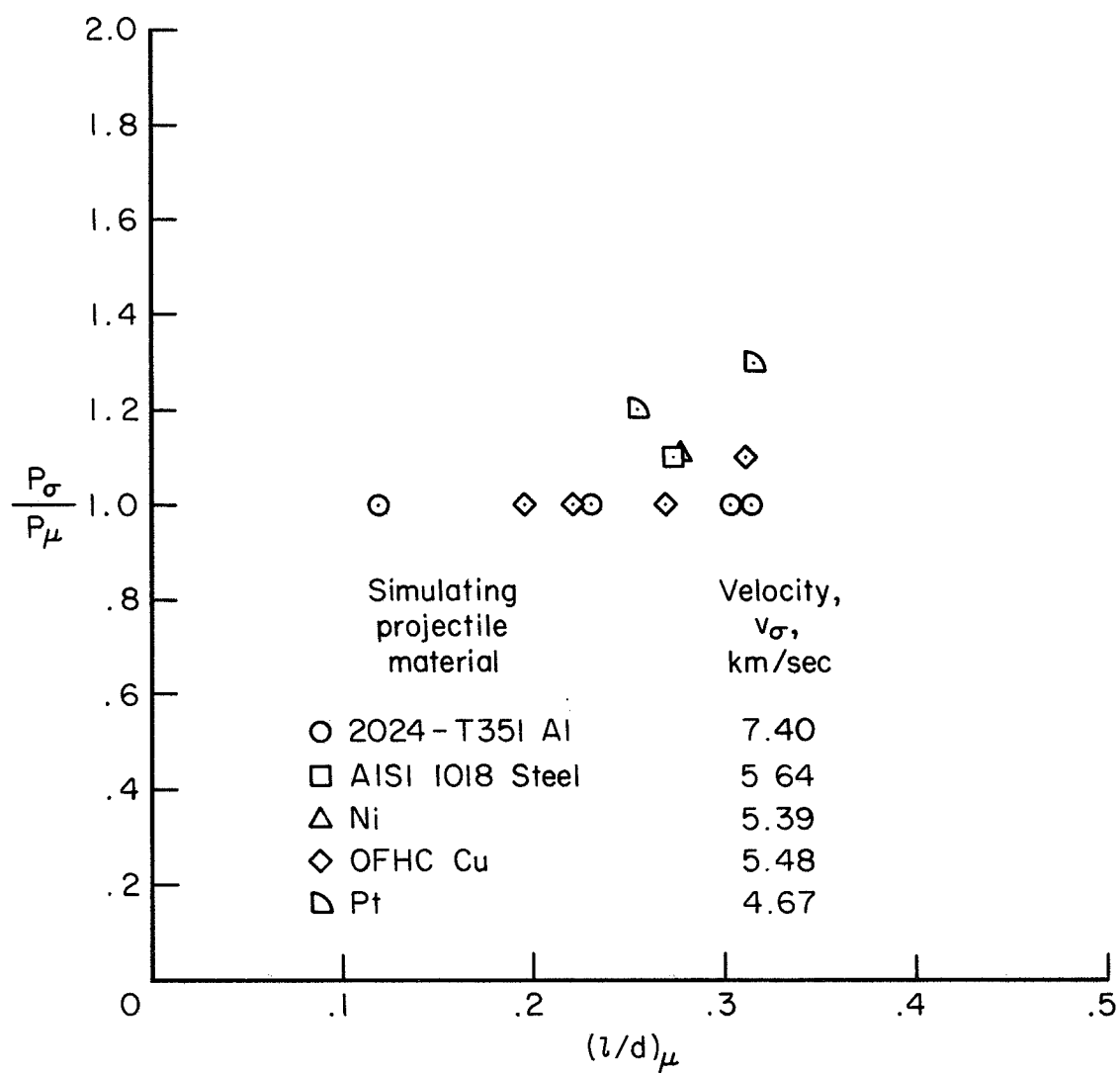Figure 3.- Wave diagram for material and wave motions occurring along x axis.

Figure 4.- Normalized penetration of simulating projectile versus fineness ratio of corresponding polyethylene cylinder impacting at 11.3 km/sec.
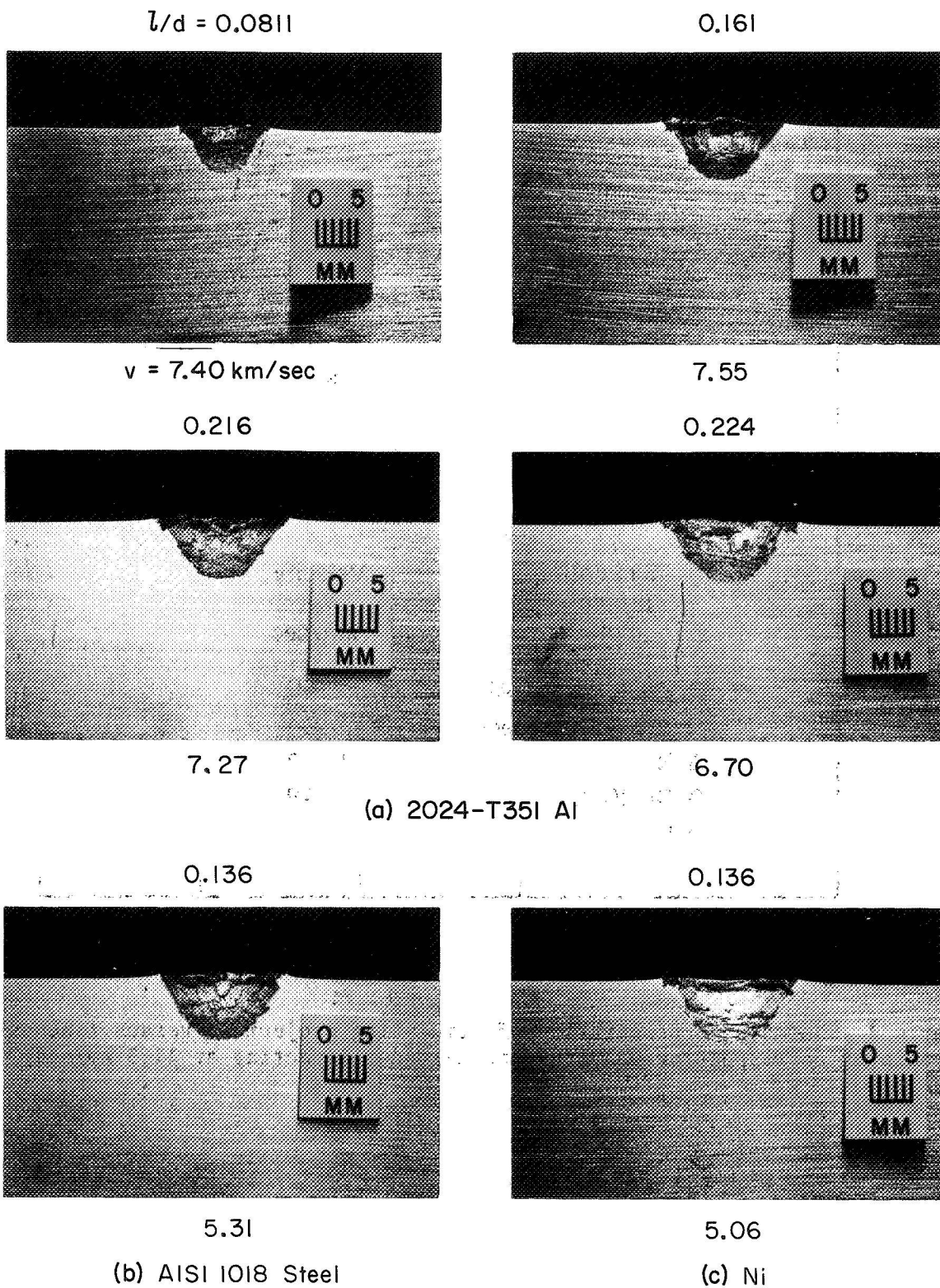
Figure 5.- Impact craters in 2024-T351 aluminum targets produced by simulating projectiles at Hugoniot pressures near 1.05 megabars.

$l/d = 0.0905$ 0.102

$v = 5.17$ km/sec   5.44

0.131   0.151

5.28   5.42

(d) OFHC Cu

0.0933   0.122
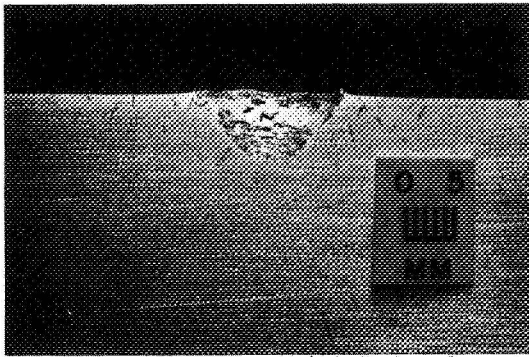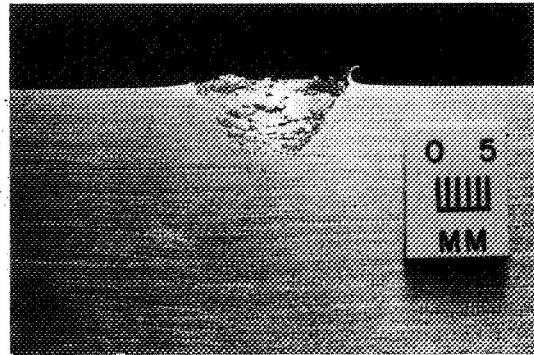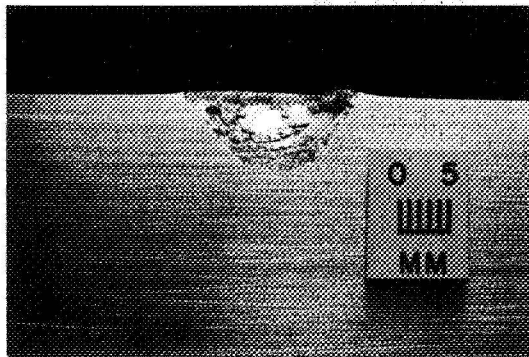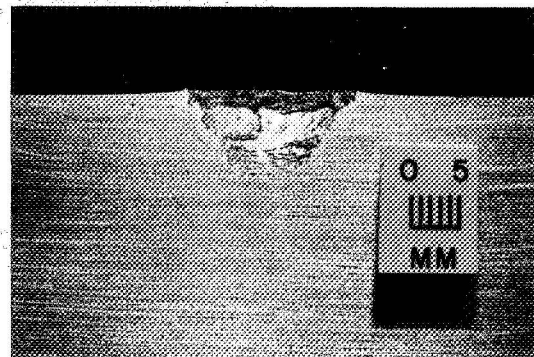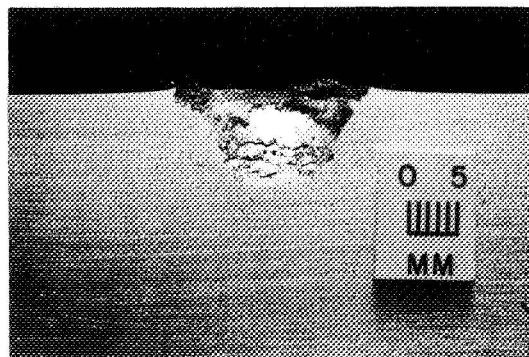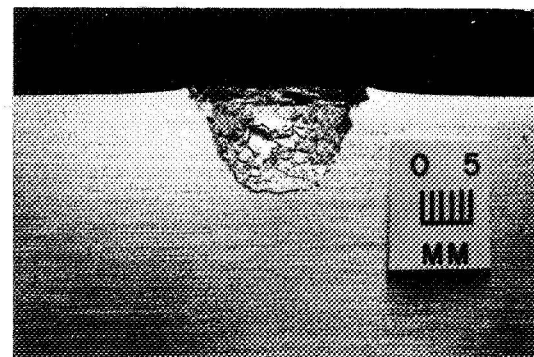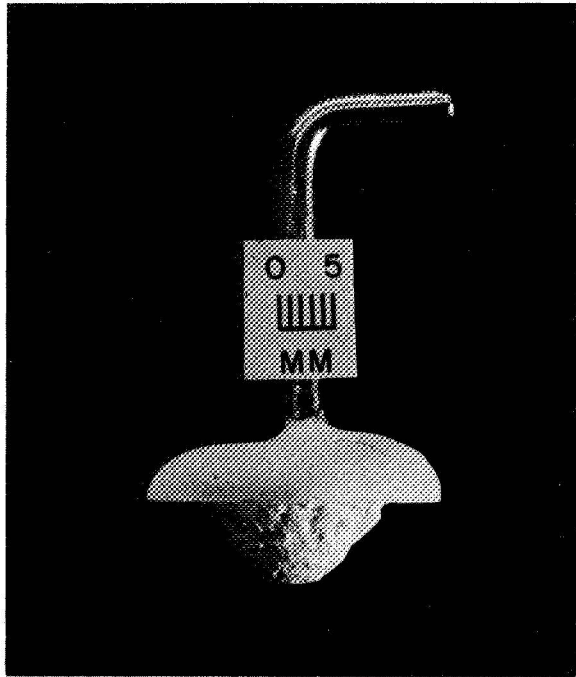
4.70   4.69

(e) Pt

Figure 5.- Concluded.

Figure 6.- Plaster replica (from ref. 2) of impact crater in 2024-T351 aluminum target produced by 1/3-fineness-ratio polyethylene cylinder at 11.3 km/sec.
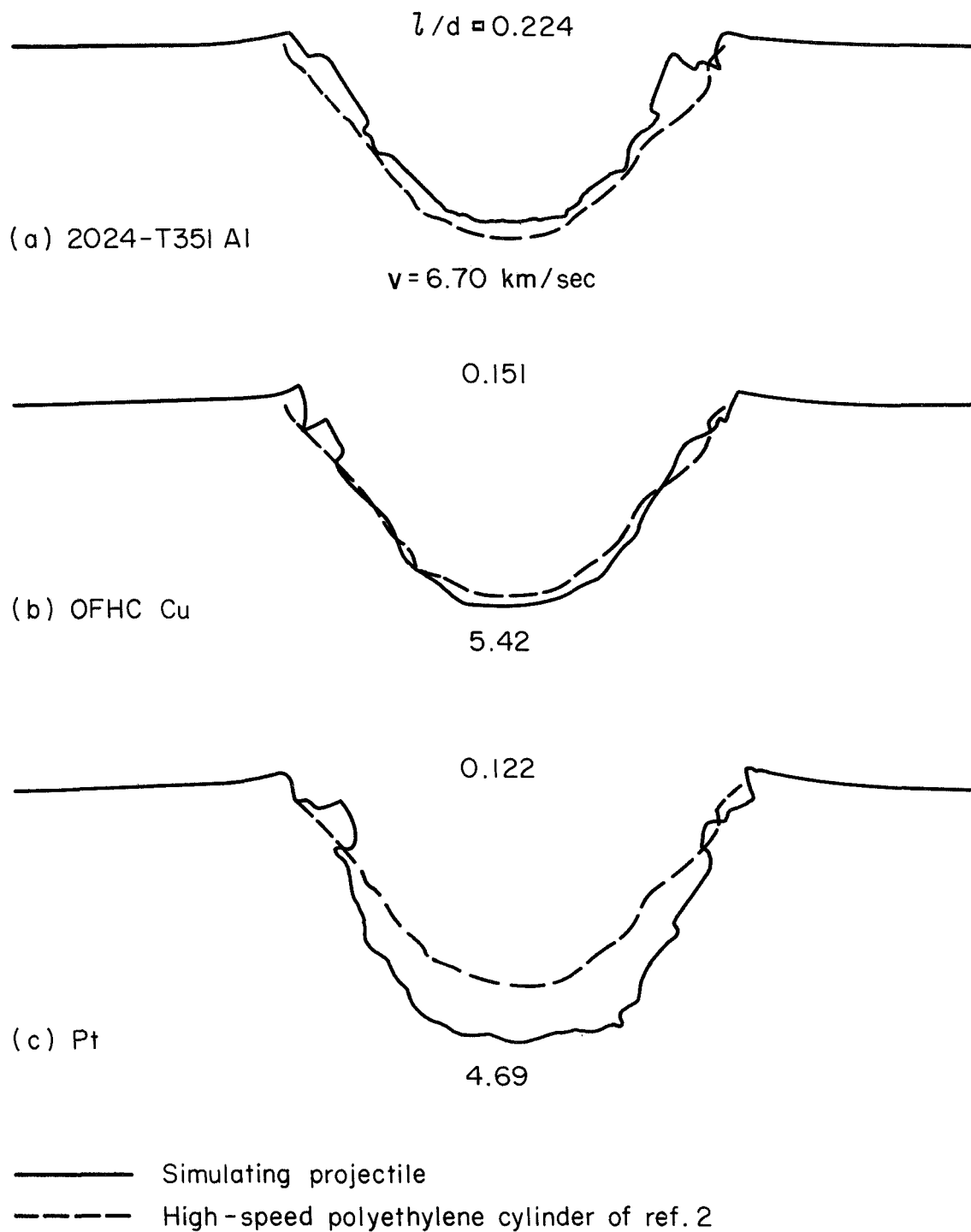
$l/d = 0.224$

(a) 2024-T351 Al

v = 6.70 km/sec

0.151

(b) OFHC Cu

5.42

0.122

(c) Pt

4.69

————— Simulating projectile

————— High-speed polyethylene cylinder of ref. 2

Figure 7.- Comparison of crater profiles.

$l/d = 0.151$

$v = 7.82$ km/sec

Figure 8.- Impact crater in 2024-T351 aluminum target produced by copper simulating projectile at Hugoniot pressure near 1.70 megabars.

"The aeronautical and space activities of the United States shall be conducted so as to contribute . . . to the expansion of human knowledge of phenomena in the atmosphere and space. The Administration shall provide for the widest practicable and appropriate dissemination of information concerning its activities and the results thereof."

— NATIONAL AERONAUTICS AND SPACE ACT OF 1958

NASA SCIENTIFIC AND TECHNICAL PUBLICATIONS

TECHNICAL REPORTS: Scientific and technical information considered important, complete, and a lasting contribution to existing knowledge.

TECHNICAL NOTES: Information less broad in scope but nevertheless of importance as a contribution to existing knowledge.

TECHNICAL MEMORANDUMS: Information receiving limited distribution because of preliminary data, security classification, or other reasons.

CONTRACTOR REPORTS: Scientific and technical information generated under a NASA contract or grant and considered an important contribution to existing knowledge.

TECHNICAL TRANSLATIONS: Information published in a foreign language considered to merit NASA distribution in English.

SPECIAL PUBLICATIONS: Information derived from or of value to NASA activities. Publications include conference proceedings, monographs, data compilations, handbooks, sourcebooks, and special bibliographies.

TECHNOLOGY UTILIZATION PUBLICATIONS: Information on technology used by NASA that may be of particular interest in commercial and other non-aerospace applications. Publications include Tech Briefs, Technology Utilization Reports and Notes, and Technology Surveys.

Details on the availability of these publications may be obtained from:

SCIENTIFIC AND TECHNICAL INFORMATION DIVISION

NATIONAL AERONAUTICS AND SPACE ADMINISTRATION
Washington, D.C. 20546